

Dipole-pion cross section in the saturation regime

G.R. Boroun*

Physics Department, Razi University, Kermanshah 67149, Iran

B.Z. Kopeliovich†

Departamento de Física, Universidad Técnica Federico Santa María, Valparaiso, Chile

(Dated: April 18, 2025)

We analyse HERA data on leading neutron production in one-pion exchange approximation. The dipole-pion cross section as function of transverse separation \mathbf{r} at small Bjorken variable β is parameterized within the bSat model. The evolution of the dipole-pion cross section is performed applying the Laplace transformation technique. We demonstrate that geometric scaling for the dipole-pion cross section hold approximately within a wide kinematic region of rQ_s . The geometrical scaling is improved applying the evolution method. That is compared with the constituent quark picture and the color dipole BFKL expansion. The cross section saturates at large dipole sizes.

1. Introduction

The color-dipole model and dipole cross section were initially introduced in Ref.[1] to explain that the interaction eigenstates in Quantum Chromodynamics (QCD) are the eigenstates of the interaction amplitude with specific values of the transverse dipole moment. Assuming that gluons in hadrons are concentrated in small areas occupying only about 10% of the light hadron's total area can be beneficial in high-energy hadronic collisions as mentioned in Ref.[2]. This concept was further developed beyond the "frozen" dipole approximation in a perturbative manner, investigating the influence of quantum coherence effects on the transverse momentum distribution of photons and gluons radiated by a quark moving through nuclear matter in Ref.[3]. Additionally, the nonperturbative interaction for light-cone fluctuations involving quarks and gluons is discussed in Ref.[4].

In the dipole picture [5], the virtual photon γ^* splits into a quark-antiquark pair (a dipole) with virtuality Q^2 exchanged between the electron and target. The dipole, with the transverse size \mathbf{r} between the quark and antiquark, interacts with the pion cloud of the proton in the leading neutrons¹ [6, 7]. The quark and antiquark in this dipole, carry a fraction z and $1 - z$ of the photon's longitudinal momentum respectively, probe the pion cloud of the proton in the inclusive $\gamma^*\pi^*$ cross section in leading neutron events $e + p \rightarrow e' + X + n$. The leading neutron production in DIS is a method to measure the dipole cross section of the pion, $\sigma_{\text{dip}}^\pi(x, \mathbf{r})$ [8].

The cross section of $\gamma^*\pi^*$ interaction is proportional to the differential cross section for γ^*p by the following form [9]

$$\sigma^{\gamma^*\pi^*}(\hat{W}^2, Q^2) = \frac{1}{f_{\pi/p}(x_L, t)} \frac{d^2\sigma(W, Q^2, x_L, t)}{dx_L dt}, \quad (1)$$

where $f_{\pi/p}$ is the flux of pions emitted by the proton and describes the splitting of a proton into a πn system. This flux is well known and can be calculated using chiral effective theory. In the chiral approach [10], the proton is shown as a superposition of states in meson-cloud models

$$|p\rangle \rightarrow \sqrt{1-a-b}|p_0\rangle + \sqrt{a}\left(-\sqrt{\frac{1}{3}}|p_0\pi^0\rangle + \sqrt{\frac{2}{3}}|n_0\pi^+\rangle + \dots\right), \quad (2)$$

with $a = 0.24$ and $b = 0.12$. The variables in Eq.(1) are: t is four-momentum transfer squared at the proton vertex; x_L is the longitudinal momentum fraction carried by the outgoing neutron. They are related to the transverse momentum

*Electronic address: boroun@razi.ac.ir

†Electronic address: boris.kopeliovich@usm.cl

¹ The leading neutrons have been known as neutron production in deep-inelastic scattering (DIS) on a proton where neutrons carry a large fraction of the proton's longitudinal momentum in the forward direction.

of the neutron, p_T , as

$$t \simeq -\frac{p_T^2}{x_L} - (1 - x_L) \left(\frac{m_n^2}{x_L} - m_p^2 \right), \quad (3)$$

with the neutron and proton masses (i.e. m_n and m_p).

The center-of-mass (COM) energies for the photon-proton and photon-pion systems are denoted by W and \hat{W} respectively, where $\hat{W}^2 = (1 - x_L)W^2$.

The dipole framework has been extended by authors in Refs.[11–14] and saturated by parametrization models in Refs.[15–17]. The total $\gamma^*\pi^*$ cross section, using the optical theorem, is related to the dipole-pion cross section as

$$\sigma_{L,T}^{\gamma^*\pi^*}(\beta, Q^2) = \int d^2\mathbf{r} \int_0^1 \frac{dz}{4\pi} |\Psi_{L,T}^f(\mathbf{r}, z; Q^2)|^2 \sigma_{\text{dip}}^{\pi}(\beta, \mathbf{r}), \quad (4)$$

where $\Psi_{L,T}(\mathbf{r}, z; Q^2)$ are the appropriate spin averaged light-cone wave functions of the photon, which give the probability for the occurrence of a $(q\bar{q})$ fluctuation of transverse size with respect to the photon polarization [18]. The Bjorken variable scaled for the photon-pion system is given by

$$\beta = \frac{Q^2 + m_f^2}{\hat{W}^2 + Q^2} = \frac{Q^2 + m_f^2}{(1 - x_L)W^2 + Q^2}, \quad (5)$$

where m_f is the active quark mass defined by the mass of the charm quark with the number of active flavors $n_f = 4$. The dipole-virtual pion cross section was proposed by the GBW model [15] as

$$\sigma_{\text{dip}}^{\pi}(\beta, \mathbf{r}) = \sigma_0 \left(1 - e^{-r^2 Q_s^2(\beta)/4} \right), \quad (6)$$

where $Q_{\text{sat}}(\beta)$ plays the role of saturation and is defined by the form $Q_{\text{sat}}^2(\beta) = Q_0^2(x_0/\beta)^\lambda$ with $Q_0^2 = 1 \text{ GeV}^2$. The geometric scaling [19] implies that the pion cross section depends only on one dimensionless variable $rQ_s(\beta)$ (for all values of r and β), as shown by

$$\sigma_{\text{dip}}^{\pi}(\beta, r) = \sigma_{\text{dip}}^{\pi}(rQ_s(\beta)). \quad (7)$$

The pion cross section can be defined by the following form

$$\sigma_{\text{dip}}^{\pi}(\beta, r) = \int d^2b \frac{d\sigma_{\text{dip}}^{\pi}}{d^2b}, \quad (8)$$

which contains all information about the target and the strong interaction physics with the impact parameter (IP), b . The dipole pion cross section at a given impact parameter b (bSat model (or IP-Sat model) [16, 17]) contains the DGLAP equation [20–22]) for the evolution of the gluon density at large scales:

$$\frac{d\sigma_{\text{dip}}^{\pi}}{d^2b}(\mathbf{b}, \mathbf{r}, \beta) = 2 \left[1 - \exp\left(-\frac{\pi^2 r^2 \alpha_s(\mu^2) \beta g(\beta, \mu^2) T_{\pi}(\mathbf{b})}{2N_c}\right) \right], \quad (9)$$

with $N_c = 3$, $\mu^2 = C/r^2 + \mu_0^2$ where μ^2 is the hard scale, and the parameters C and μ_0^2 are obtained from the fit to the DIS data as summarized in [7, 23]. The Gaussian form of the function $T_{\pi}(\mathbf{b})$ is determined from the fit to the data as

$$T_{\pi}(\mathbf{b}) = \frac{1}{2\pi B_{\pi}} \exp\left(-\frac{b^2}{2B_{\pi}}\right). \quad (10)$$

The parameter B_{π} is the width of the pion and is chosen to be $B_{\pi} = 2 \text{ GeV}^{-2}$ from the Belle measurements [24]. Since the free parameters depend on the leading neutron structure function data or the inclusive proton data, we can consider the ratio of dipole cross sections at small x given by

$$R_q = \frac{\sigma_{\text{dip}}^{\pi}(r, \beta)}{\sigma_{\text{dip}}^p(r, \beta)}, \quad (11)$$

or

$$R_q = \frac{\frac{d\sigma_{\text{dip}}^\pi(\mathbf{b}, \mathbf{r}, \beta)}{d^2b}}{\frac{d\sigma_{\text{dip}}^p(\mathbf{b}, \mathbf{r}, \beta)}{d^2b}}. \quad (12)$$

In a constituent quark picture and the color dipole BFKL-Regge expansion model [25], R_q represents the ratio of valence quarks in the pion and proton i.e., $R_q = \frac{2}{3}$. The value $R_q = \frac{1}{2}$ is acceptable as studied in Ref.[8]. In this paper, we aim to evolve the dipole-pion cross section using a Laplace transform technique in terms of the known initial condition.

2. Formalism

The color dipole-pion cross section in the bSat model is given by

$$\frac{d\sigma_{\text{dip}}^\pi(\mathbf{b}, \mathbf{r}, \beta)}{d^2b} = 2 \left[1 - \exp(-F_{\text{DGLAP}}(\mathbf{b}, \mathbf{r}, \beta)) \right], \quad (13)$$

where

$$F_{\text{DGLAP}}(\mathbf{b}, \mathbf{r}, \beta) = \frac{\pi^2 r^2 \alpha_s(\mu^2) \beta g(\beta, \mu^2) T_\pi(\mathbf{b})}{2N_c}. \quad (14)$$

The function F_{DGLAP} applies in the DGLAP evolution equation where the gluon density is dominant at low x . Therefore we find

$$\begin{aligned} \frac{\partial F_{\text{DGLAP}}(\mathbf{b}, \mathbf{r}, \beta)}{\partial r} &= -\alpha_s(\mu^2) r^2 \frac{\partial}{\partial r} \left(\frac{1}{\alpha_s(\mu^2) r^2} \right) F_{\text{DGLAP}}(\mathbf{b}, \mathbf{r}, \beta) - \frac{2C}{r^3 \mu^2} \int_\beta^1 \frac{\beta}{\gamma^2} d\gamma \sum_{n=1} \left(\frac{\alpha_s(\mu^2)}{2\pi} \right)^{(n)} \\ &\times P_{gg}^{(n)} \left(\frac{\beta}{\gamma} \right) F_{\text{DGLAP}}(\mathbf{b}, \mathbf{r}, \gamma), \end{aligned} \quad (15)$$

where n is the order of α_s . After some rearranging, we find an evolution equation in terms of r

$$\begin{aligned} dF_{\text{DGLAP}}(\mathbf{b}, \mathbf{r}, \beta) &= F_{\text{DGLAP}}(\mathbf{b}, \mathbf{r}, \beta) \left[\frac{2}{r} + \frac{d \ln \alpha_s(r)}{dr} \right] dr - \frac{2C}{r^3 \left(\frac{C}{r^2} + \mu_0^2 \right)} dr \int_\beta^1 \frac{\beta}{\gamma^2} d\gamma \sum_{n=1} \left(\frac{\alpha_s(\mu^2)}{2\pi} \right)^{(n)} \\ &\times P_{gg}^{(n)} \left(\frac{\beta}{\gamma} \right) F_{\text{DGLAP}}(\mathbf{b}, \mathbf{r}, \gamma). \end{aligned} \quad (16)$$

We can rewrite the above evolution equation of the dipole-pion cross section in the bSat model in terms of the variables $v = \ln(1/\beta)$ and r instead of β and r using the notation $\hat{F}_{\text{DGLAP}}(\mathbf{b}, v, r) \equiv F_{\text{DGLAP}}(\mathbf{b}, e^{-v}, r)$ as

$$\begin{aligned} d\hat{F}_{\text{DGLAP}}(\mathbf{b}, v, r) &= \hat{F}_{\text{DGLAP}}(\mathbf{b}, v, r) \left[\frac{2}{r} + \frac{d \ln \alpha_s(r)}{dr} \right] dr - \frac{2C}{r^3 \left(\frac{C}{r^2} + \mu_0^2 \right)} dr \int_0^v e^{-(v-w)} \sum_{n=1} \left(\frac{\alpha_s(\mu^2)}{2\pi} \right)^{(n)} \\ &\times P_{gg}^{(n)}(v-w) \hat{F}_{\text{DGLAP}}(\mathbf{b}, r, w) dw, \end{aligned} \quad (17)$$

By using the Laplace transform method developed in detail in [26–30] as $\mathcal{L}[\hat{F}_{\text{DGLAP}}(\mathbf{b}, v, r); s] \equiv F_{\text{DGLAP}}(\mathbf{b}, s, r)$ and the fact that the Laplace transform of a convolution factors is simply the ordinary product of the Laplace transform of the factors, we find

$$F_{\text{DGLAP}}(\mathbf{b}, s, r) = F_{\text{DGLAP}}(\mathbf{b}, s, r_0) \left(\frac{r}{r_0} \right)^2 \frac{\alpha_s(r)}{\alpha_s(r_0)} \exp \left[- \int_{r_0}^r \frac{2C}{\xi^3 \left(\frac{C}{\xi^2} + \mu_0^2 \right)} \sum_{n=1} \left(\frac{\alpha_s(\xi)}{2\pi} \right)^{(n)} h_{gg}^{(n)}(s) d\xi \right]. \quad (18)$$

To find the inverse the Laplace transform of the factors, we find that

$$\hat{F}_{\text{DGLAP}}(\mathbf{b}, v, r) = \int_0^v \hat{\eta}(\mathbf{b}, w, r, r_0) \hat{J}(v - w, \alpha_s(r)) dw, \quad (19)$$

where

$$\hat{\eta}(\mathbf{b}, v, r, r_0) = \hat{F}_{\text{DGLAP}}(\mathbf{b}, v, r_0) \left(\frac{r}{r_0} \right)^2 \frac{\alpha_s(r)}{\alpha_s(r_0)}. \quad (20)$$

The inverse Laplace transform of the coefficients $h_{gg}^{(n)}(s)$ in Eq. (18) is straightforward, if we keep the $1/s$ terms of the coefficients at the high-energy region as

$$\hat{J}(v, \alpha_s(r)) = \delta(v) + \frac{\sqrt{-\phi}}{\sqrt{v}} I_1(2\sqrt{-\phi}\sqrt{v}), \quad (21)$$

where²

$$\phi = \frac{2C_A}{2\pi} \int_{r_0}^r \frac{2C\alpha_s(r)}{r^3 \left(\frac{C}{r^2} + \mu_0^2 \right)} dr + \frac{(12C_F T_f - 46C_A T_f)}{9(2\pi)^2} \int_{r_0}^r \frac{2C\alpha_s^2(r)}{r^3 \left(\frac{C}{r^2} + \mu_0^2 \right)} dr, \quad (22)$$

with $C_F = \frac{N_c^2 - 1}{2N_c}$, $T_f = \frac{1}{2}n_f$ and $C_A = 3$. Transforming back in to β space, $F_{\text{DGLAP}}(\mathbf{b}, \beta, r)$ is given by

$$F_{\text{DGLAP}}(\mathbf{b}, \beta, r) = \left(\frac{r}{r_0} \right)^2 \frac{\alpha_s(r)}{\alpha_s(r_0)} \left[F_{\text{DGLAP}}(\mathbf{b}, \beta, r_0) + \int_{\beta}^1 F_{\text{DGLAP}}(\mathbf{b}, \gamma, r_0) \frac{\sqrt{-\phi}}{\sqrt{\ln \frac{\gamma}{\beta}}} I_1(2\sqrt{-\phi}\sqrt{\ln \frac{\gamma}{\beta}}) \frac{d\gamma}{\gamma} \right], \quad (23)$$

where

$$F_{\text{DGLAP}}(\mathbf{b}, \beta, r_0) = \frac{\pi^2 r_0^2 \alpha_s(r_0) \beta g(\beta, r_0) T_{\pi}(\mathbf{b})}{2N_c}, \quad (24)$$

and the initial gluon distribution at the scale $\mu_0^2 = 1.1 \text{ GeV}^2$ is defined in the form [7]

$$\beta g(\beta, \mu_0^2) = A_g \beta^{-\lambda_g} (1 - \beta)^6, \quad (25)$$

where parameters in the bSat model are motivated by the leading neutron structure function HERA data for $\beta \leq 0.01$ [6, 7]. Therefore, the evolution of the color dipole-pion cross section in the bSat model is defined by the following form

$$\frac{1}{2} \frac{d\sigma_{\text{dip}}^{\pi}}{d^2b}(\mathbf{b}, \mathbf{r}, \beta) = 1 - \exp \left\{ - \left(\frac{r}{r_0} \right)^2 \frac{\alpha_s(r)}{\alpha_s(r_0)} \left[F_{\text{DGLAP}}(\mathbf{b}, \beta, r_0) + \int_{\beta}^1 F_{\text{DGLAP}}(\mathbf{b}, \gamma, r_0) \frac{\sqrt{-\phi}}{\sqrt{\ln \frac{\gamma}{\beta}}} I_1(2\sqrt{-\phi}\sqrt{\ln \frac{\gamma}{\beta}}) \frac{d\gamma}{\gamma} \right] \right\}. \quad (26)$$

3. Results and Conclusion

The free parameters for the pion and proton are chosen from the fit results in Refs.[7, 23, 31], as summarized in Table I. The QCD parameter Λ for four active flavors has been determined as $\alpha_s(M_z^2) = 0.1166$ resulting in $\Lambda_{nf=4}^{\text{LO}} = 136.8 \text{ MeV}$ and $\Lambda_{nf=4}^{\text{NLO}} = 284.0 \text{ MeV}$. The dipole-pion cross section results in the bSat model are derived from an exclusive measurement of $e + p \rightarrow e + J/\Psi + \pi + n$ as

$$\beta = \frac{\mu^2 + m_c^2}{(1 - x_L)W^2 + \mu^2}, \quad (27)$$

² $I_1(x)$ is the Bessel function.

TABLE I: Free parameters for pion [7, 23] and proton [31].

---	A_g	λ_g	C	μ_0^2 [GeV ²]	B [GeV ⁻²]
Proton	1.350	0.079	0.380	1.73	4.0
Pion	1.208	0.060	1.453	1.10	2.3

TABLE II: Minimum values of R_q into r ($0.01 < r < 0.07$ fm)

Min	β	$b = 0$ GeV ⁻¹	$b = 2$ GeV ⁻¹
R_q	10^{-2}	~ 0.61	~ 0.42
R_q	10^{-4}	~ 0.68	~ 0.47

where $m_c = 1.3$ GeV and $x_L = 0.6$, with the Bjorken scaling in the photon-proton scattering in the dipole picture given by

$$x = \frac{(\mu^2 + m_c^2)\beta(1 - x_L)}{(1 - \beta x_L)\mu^2 + m_c^2}. \quad (28)$$

Table I displays the free parameters for the pion [7, 23] and proton [31]. The dipole-pion cross sections, $\frac{d\sigma_{\text{dip}}^\pi}{2d^2b}$, are plotted in Fig.1 over a wide range of the dipole size r in the bSat model at different values of the scaled Bjorken variable $\beta = 10^{-2}$ and 10^{-4} with the impact parameters $b = 0$ and 2 GeV⁻¹. In Fig.1 (left-hand side), the dipole-pion cross sections are shown at $\beta = 10^{-2}$ (upper panel) and $\beta = 10^{-4}$ (lower panel) as a function of dipole size r . The dipole-pion cross sections saturate for large dipole sizes and increase towards lower dipole sizes as the Bjorken scaling decreases. The impact parameters (i.e., $b = 0$ and 2 GeV⁻¹) affect the dipole-pion cross sections at various values of r . In Fig.1 (right-hand side), the dipole-pion cross sections in the bSat model converge into a single curve when plotted against the dimensionless variable rQ_s . The saturation formalism of the dipole-pion cross section leads to improved results³ due to the evolution of the cross section becoming a function of a single variable, rQ_s , for almost all values of r with different β at $b = 0$ and 2 GeV⁻¹ in the bSat model. This evolution improves the breaking of geometrical scaling as predicted in Ref.[7].

The values of R_q predicted from the ratio $\frac{d\sigma_{\text{dip}}^\pi(\mathbf{b}, \mathbf{r}, \beta)}{d^2b} / \frac{d\sigma_{\text{dip}}^p(\mathbf{b}, \mathbf{r}, \beta)}{d^2b}$ in a wide range of the dipole size r in the bSat model at different values of the scaled Bjorken variable $\beta = 10^{-2}$ and 10^{-4} with impact parameters $b = 0$ and 2 GeV⁻¹ are illustrated in Fig.2. This ratio is running in a wide range of the dipole size r [7, 8] and it is independent of β at large and low values of r (left panel of Fig.2). We observe that the saturation scale increases towards the low values of r as β decreases. The behavior of R_q depends on the impact parameter b at small values of r and saturates at large values of r . The minimum values of R_q are obtained due to the β and b values in Table II.

In Fig.2 (left-hand side), R_q is plotted at $\beta = 10^{-2}$ (upper panel) and $\beta = 10^{-4}$ (lower panel) as a function of dipole size r . R_q saturates at large dipole sizes, with saturation increasing towards lower dipole sizes as the Bjorken scaling decreases. In Fig.2 (right-hand side), we observe that the behavior of R_q is plotted independently of β at both large and small values of r for the impact parameters $b = 0$ (upper) and 2 GeV⁻¹ (lower). This value depends on β at moderate r ($2 \times 10^{-2} \lesssim r \lesssim 7 \times 10^{-1}$ fm) as the impact parameter increases.

In conclusion, we have presented the evolution of the dipole-pion cross section based on the Laplace transform method in the bSat model as a function of the dipole size and the scaled Bjorken variable β . The evolution model can successfully describe the leading neutron data in terms of the impact parameter at small β (Fig.1, left). The scaling behavior in the bSat model is shown at large and small dipole sizes, similar to the GBW model. These results in rQ_s (Fig.1, right), which are independent of the impact parameter and the scaled Bjorken variable, show that the evolution effects play a dominant role in the leading neutron DIS cross section.

The ratio R_q in the bSat model depends on the impact parameter at small dipole size and is scaled at large dipole sizes (Fig.2). This ratio varies between the values $0.4 < R_q \leq 1$ over a wide range of r . The behavior of the ratio R_q over this range of r depends on the structure of the proton, from the valence quarks to a multiquark in the proton.

³ An important property of the saturation formalism is the geometric scaling phenomenon, which means that the scattering amplitude and corresponding cross sections can scale on the dimensionless scale rQ_s .

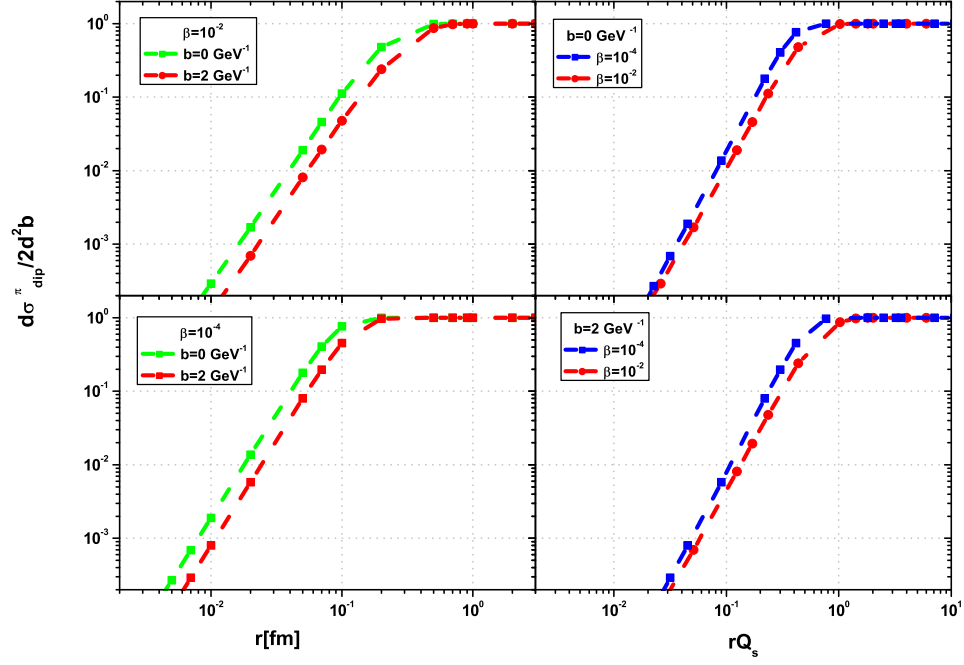


FIG. 1: Dipole-pion cross section in the bSat model as a function of r (left panel) and rQ_s (right panel) for $\beta = 10^{-2}$ and 10^{-4} at the impact parameters $b = 0$ and 2 GeV^{-1} . Left panel (upper): $\beta = 10^{-2}$ and $b = 0 \text{ GeV}^{-1}$ (green-square) and $b = 2 \text{ GeV}^{-1}$ (red-circle). Left panel (lower): $\beta = 10^{-4}$ and $b = 0 \text{ GeV}^{-1}$ (green-square) and $b = 2 \text{ GeV}^{-1}$ (red-circle). Right panel (upper): $b = 0 \text{ GeV}^{-1}$ and $\beta = 10^{-4}$ (blue-square) and $\beta = 10^{-2}$ (red-circle). Right panel (lower): $b = 2 \text{ GeV}^{-1}$ and $\beta = 10^{-4}$ (blue-square) and $\beta = 10^{-2}$ (red-circle).

Quantum fluctuations in the proton at small dipole interact with the quarks and antiquarks in the meson cloud of the proton, depending on the flavor asymmetric and flavor symmetric sea [8].

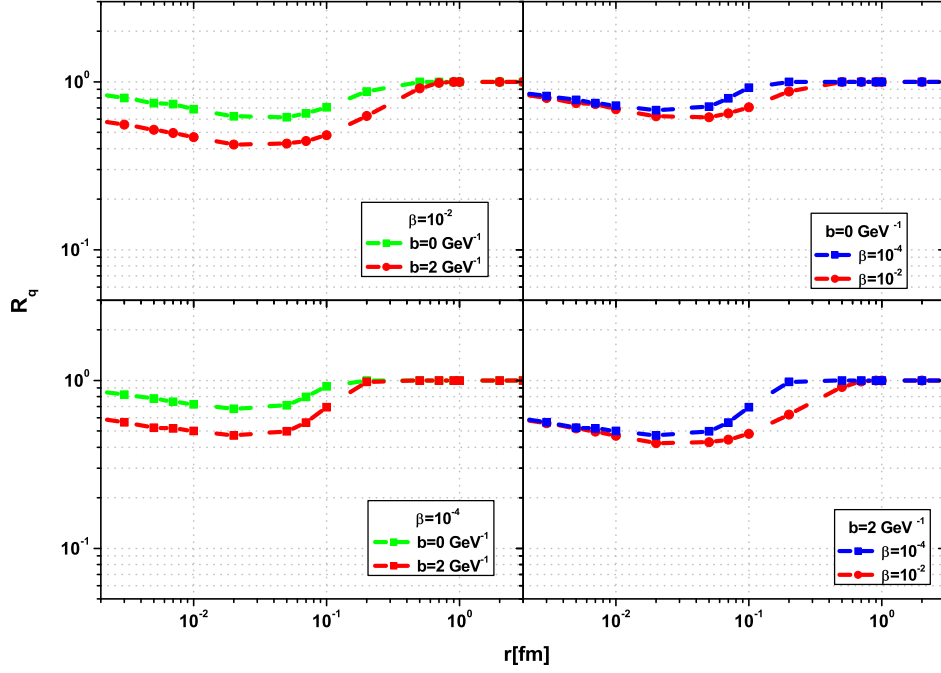


FIG. 2: The ratio $R_q = \frac{d\sigma_{\text{dip}}^{\pi}(\mathbf{b}, \mathbf{r}, \beta)}{d^2b} / \frac{d\sigma_{\text{dip}}^p(\mathbf{b}, \mathbf{r}, \beta)}{d^2b}$ is plotted as a function of r for $\beta = 10^{-2}$ and 10^{-4} at the impact parameters $b = 0$ and 2 GeV^{-1} . Left panel (upper): $\beta = 10^{-2}$ and $b = 0 \text{ GeV}^{-1}$ (green-square) and $b = 2 \text{ GeV}^{-1}$ (red-circle). Left panel (lower): $\beta = 10^{-4}$ and $b = 0 \text{ GeV}^{-1}$ (green-square) and $b = 2 \text{ GeV}^{-1}$ (red-circle). Right panel (upper): $b = 0 \text{ GeV}^{-1}$ and $\beta = 10^{-4}$ (blue-square) and $\beta = 10^{-2}$ (red-circle). Right panel (lower): $b = 2 \text{ GeV}^{-1}$ and $\beta = 10^{-4}$ (blue-square) and $\beta = 10^{-2}$ (red-circle).

-
- [1] A.B. Zamolodchikov, B.Z. Kopeliovich and L.I. Lapidus, *Pis'ma Zh. Eksp. Teor. Fiz.* **33**, 612 (1981); *Sov. Phys. JETP Lett.* **33**, 595 (1981).
 - [2] B. Z. Kopeliovich, I. K. Potashnikova, B. Povh and I. Schmidt, *Phys. Rev. D* **76**, 094020 (2007).
 - [3] B.Z. Kopeliovich, A. Schäfer and A.V. Tarasov, *Phys. Rev. C* **59**, 1609 (1999).
 - [4] B.Z. Kopeliovich, A. Schäfer and A.V. Tarasov, *Phys. Rev. D* **62**, 054022 (2000).
 - [5] N. N. Nikolaev and B. G. Zakharov, *Phys. Lett. B* **332**, 184 (1994).
 - [6] A.Kumar and T.Toll, *Phys.Rev.D* **105**, 114045 (2022).
 - [7] A.Kumar, *Phys.Rev.D* **107**, 034005 (2023).
 - [8] B. Z. Kopeliovich, I. K. Potashnikova, B. Povh and I. Schmidt, *Phys. Rev. D* **85**, 114025 (2012).
 - [9] F. Carvalho et al., *Phys. Lett. B* **752**, 76 (2016).
 - [10] A.W. Thomas, W.Melnitchouk and F.M.Steffens, *Phys.Rev.Lett.* **85**, 2892 (2000).
 - [11] V. P. Goncalves, F. S. Navarra and D. Spiering, *Phys. Rev. D* **93**, 054025 (2016).
 - [12] F. Carvalho, V. P. Goncalves, F. S. Navarra and D. Spiering, *Phys. Rev. D* **103**, 034021 (2021).
 - [13] J. T. Amaral and V. M. Becker, *Phys. Rev. D* **97**, 094026 (2018).
 - [14] B. Z. Kopeliovich, I. K. Potashnikova and Ivan Schmidt, *Phys.Rev.C* **81**, 035204 (2010).
 - [15] K.Golec-Biernat and M.Wüsthoff, *Phys. Rev. D* **59**, 014017 (1998).
 - [16] H. Kowalski and D. Teaney, *Phys. Rev. D* **68**, 114005 (2003).
 - [17] H. Kowalski, L. Motyka and G. Watt, *Phys. Rev. D* **74**, 074016 (2006).
 - [18] J. T. Amaral, D. A. Fagundes and M. V. T. Machado, *Phys. Rev. D* **103**, 016013 (2021).
 - [19] A. M. Stasto, K. J. Golec-Biernat and J. Kwiecinski, *Phys. Rev. Lett.* **86**, 596 (2001).
 - [20] Yu.L.Dokshitzer, *Sov.Phys.JETP* **46**, 641 (1977).
 - [21] G.Altarelli and G.Parisi, *Nucl.Phys.B* **126**, 298 (1977).
 - [22] V.N.Gribov and L.N.Lipatov, *Sov.J.Nucl.Phys.* **15**, 438 (1972).

- [23] H. Mäntysaari and P. Zurita, Phys. Rev. D **98**, 036002 (2018).
- [24] S. Uehara, et al., Phys. Rev. D **86**, 092007 (2012); M. Masuda, et al., Phys. Rev. D **93**, 032003 (2016).
- [25] N. Nikolaev, J. Speth and V. Zoller, Phys.Lett.B **473**, 157 (2000).
- [26] Martin M. Block, Loyal Durand, and Douglas W. McKay, Phys. Rev. D **79**, 014031 (2009).
- [27] Martin M. Block, Loyal Durand, Phuoc Ha, and Douglas W. McKay, Phys. Rev. D **83**, 054009 (2011).
- [28] Martin M. Block, Loyal Durand, Phuoc Ha, and Douglas W. McKay, Phys. Rev. D **84**, 094010 (2011).
- [29] Martin M. Block, Loyal Durand, Phuoc Ha, and Douglas W. McKay, Phys. Rev. D **88**, 014006 (2013).
- [30] G.R.Boroun and Phuoc Ha, Phys. Rev. D **109**, 094037 (2024).
- [31] K. Golec-Biernat and S.Sapeta, JHEP **03**, 102 (2018).